FLOMEKO 2022

Transferability of calibration results obtained with conventional gases for application with hydrogen

B. Mickan[1], H.-B. Böckler[2], D. Schumann[3], J. van der Grinten[4]

[1]Physikalisch-Technische Bundesanstalt, bodo.mickan@ptb.de, Braunschweig, Germany
[2]Physikalisch-Technische Bundesanstalt, hans-benjamin.boeckler@ptb.de, Braunschweig, Germany
[3]Physikalisch-Technische Bundesanstalt, daniel.schumann@ptb.de, Braunschweig, Germany
[4]Physikalisch-Technische Bundesanstalt, jos.v.grinten @ptb.de, Braunschweig, Germany
E-mail (corresponding author): bodo.mickan@ptb.de

Abstract

In the field of gas transport, the de-carbonisation of the energy supply is forcing the exchange of natural gas with hydrogen, either in mixtures or even pure hydrogen. Therefore, there is an increasing need to have reliable information about the behaviour of existing metering technologies with such hydrogen enriched gases or pure hydrogen. On the other hand, the availability of testing and calibration infrastructures for hydrogen has been very limited so far. A fast approach to close this gap is the usage of scaling procedures to transfer the calibration results gathered at facilities with conventional gases to field applications with hydrogen.
The paper will introduce the scaling models applied at PTB for turbine gas meters (TM), rotary piston gas meters (RM) and differential pressure meters (DPM) to ensure transferability of calibration results obtained mainly with air and natural gas, and occasionally with nitrogen or water. All applied models are based on the Reynolds number as the dominant scaling parameter and include extensions to describe secondary effects if necessary.

1. Introduction

The expected change from natural gas to hydrogen in large scales is already forcing the activities of transport grid operators and meter manufacturers to prepare their infrastructure and technologies for the upcoming needs. Therefore, there is also a need of new test infrastructure with reliable traceability to the SI units. The PTB as a NMI has been already requested to establish such traceability for the test facilities at DNV[1] and RMA[2] for hydrogen enriched gases and pure hydrogen as well for large scale flows of up to 6500 m^3/h and pressures up to 52 bar.

The main approach of PTB to provide traceability with low uncertainty for different gases is the usage of critical flow venturi nozzles (CFVN) as it is described in [1]. But there is also a need to establish the valid calibration of conventional working or transfer standards such as e.g. turbine meters, either in situations where the facilities does not allow the usage of CFVNs, for comparison purpose on site or directly for custody transfer.

The paper presents the theoretical background used by PTB to establish transferability for fluids others than air and natural gas for turbine meters, rotary meters and differential pressure meters. The basics equations for meters deviation resp. calibration characteristic are introduced, examples will be shown, and some aspects of the transferability are discussed.

2. Turbine Meters (TM)

The fact that the meter deviation of turbine meters is mainly depending on Reynolds number if the momentum ρq^2 of the flow is strong enough to overrule the friction of the bearings is well known for longer time. The more detailed mathematical description of these relationships has been elaborated at PTB since 2007 and has been improved since then. There have been already successful applications and approvals in practise e.g. [2][3].

2.1 Model for meter deviation of TM

The central starting point of the development of the mathematical model for meter deviation is the general equation (1) for torques at the turbine wheel in balance with the acceleration of the wheel. In case of stationary condition, the right site of eq. (1) is finally summed up to Zero.

$$J\dot{\omega} = 0 = M_{\Delta q} + M_{\tau_w} + M_B \qquad (1)$$

The part $M_{\Delta q}$ stands for the torque what is caused by the velocity difference in the case that the rotation speed of the wheel causes a direction change of the originally axial flow in the pipe. The flow along the turbine blade itself causes a force and therefore torque $M_{\tau w}$ at the wheel due to the wall shear stress τ_w in the boundary layer at the

[1] DNV Netherlands BV, Fuel and Flow Advisory Groningen Energieweg 17, 9743AN Groningen, the Netherlands

[2] RMA Mess- und Regeltechnik GmbH & Co. KG, Calibration Rig, Forsthausstr. 3, 77866 Rheinau, Germany

blade surface. Finally, there is the friction in the bearing friction which causes an always decelerating torque M_B.

The torque $M_{\Delta q}$ due to direction change is proportional to the difference of real flow rate q and flow rate q_i indicated by the rotation frequency of the wheel as well as to the mass flow rate ρq of the flow. The torque $M_{\tau w}$ is proportional to the Reynolds depending friction factor $c_{f,Re}$ at the blade and the momentum of the flow given by ρq^2.

$$0 = C_1 \rho q (q - q_i) + C_2 \rho q^2 c_{f,Re} + M_B \qquad (2)$$

With division by $C_1 J \rho q^2$ we already get the relation to our meter deviation:

$$e_{TM} = \frac{q_i}{q} - 1 = \frac{C_2}{C_1 J} c_{f,Re} + \frac{M_B}{C_1 J \rho q^2} \qquad (3)$$

The torque M_B due to bearing friction can be expressed for bearings with Newtonian lubrification fluids in a simple linear relationship to the rotation frequency of the wheel and therefore linear to the indicated flow rate q_i.

$$M_B = a_{mb} + b_{mb} q_i \qquad (4)$$

Finally, we formulate the meter deviation of a turbine meter with the superposition of three components[3] as:

$$e_{TM} = e_{Re} + e_{MB} + e_{Ma} \qquad (5)$$

with

$$e_{Re} = \frac{C_2}{C_1 J} c_{f,Re}$$

$$e_{Ma} = c_{Ma} \frac{\rho q^2}{p}$$

$$e_{MB} = \frac{\frac{a_{20}}{\tan\beta} + b_{20} q_{i,20}}{\rho q_{20}^2} \qquad (6)$$

$$\text{and } q_{20} = \frac{q}{\frac{\pi}{4} D_N^2 \cdot 20 \frac{\text{m}}{\text{s}}};\ q_{i,20} = \frac{q_i}{\frac{\pi}{4} D_N^2 \cdot 20 \frac{\text{m}}{\text{s}}}$$

The parameters a_{mb} and b_{mb} of eq. (4) are transformed to q_{20} and b_{20} including the inclination angle β of the blades against the pipe axis and a relative flow which is related to flow speed of 20 m/s in the nominal pipe diameter of the meter. It is an outcome of the statistical analysis of larger set of meters that with this we get a quite good similarity between the meters. This will be discussed in section 2.3.

It is possible to determine the parameters a_{20} and b_{20} directly based on two specific experiments: a spin down test and a step response test. The spin down test can be done at PTB under nearly vacuum condition (≈ 300 Pa absolute pressure), so that there is no significant impact of fluid friction on the wheel present. The step response test is applying sudden flow rate changes by means of switching critical nozzles at the main air flow facility of PTB. Technical details to the arrangement of these tests can be found in [4].

2.2 Example for meter deviation of a TM

The relations between the measured meter deviation e_{TM} and the part e_{Re} is shown in Figure 1 for a G250 turbine meter with pipe size D_N = 100 mm. This meter was used in a joint industry project of DNV and details about the evaluation of traceability including this meter can be found in [3]. The meter has been calibrated at PTB with air and at DNV test facilities with natural gas[4]. The parameters for bearing friction in e_{MB} have been determined as mentioned above at PTB with spin down and step response test. Therefore, the Figure 1 shows additionally $e_{Re} = e_{TM} - e_{MB}$.

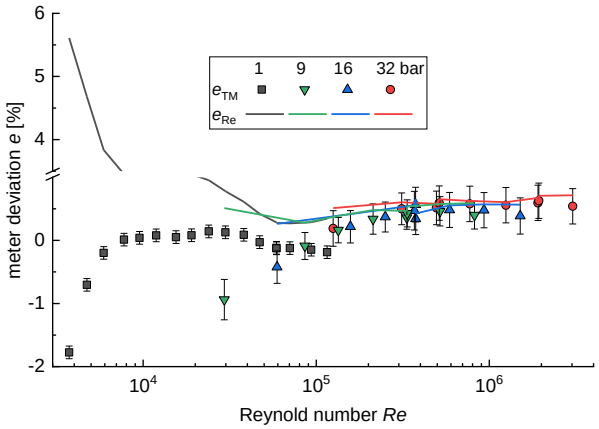

Figure 1: Example for meter deviations measured with atmospheric air and natural gas at different pressure (9 to 32 bar) of a G250/DN100. Please note the interruption of the y-axis to handle the larger span of e_{Re} at low Reynolds numbers.

The impact of the bearing, i.e. the difference between e_{TM} and e_{Re}, is remarkable especially at the lowest flow with atmospheric air. At this point we see a difference up to 7.5 %. Also, in the overlap in Reynolds of air calibration (black squares) and those with natural gas (9 bar, green triangle down), we see differences between the calibration results in order of 1 %, what exceeds the uncertainties of the measurements by factors. But in the points for e_{Re}, when e_{MB} is removed mathematically from e_{TM}, all single values of e_{Re} agree within their uncertainties (without additional uncertainty for e_{MB}!).

The points of e_{Re} can be finally approximated by an appropriate function of Reynolds number only and

[3] The third part of meter deviation e_{Ma} in eq. (5) and (6) is not yet discussed and is also not subject of the consideration in this paper. This part is expressing the influence of temperature effects and the fact that the temperature of the fluid is not measured at the wheel but somewhere in the larger cross section of the main pipe. Due to the higher speed at the wheel compared the location of the T-sensor we have a Mach effect on the temperature. This effect is only relevant at q_{max} and is usually not higher than 0.2 % for well-designed turbine meters. We are focussing on the bigger impact of M_B at low flows because of the low density of hydrogen.

[4] The facilities of DNV are traceable to the European Harmonised Reference Value via FORCE and ISO17025 accredited.

together with the parameterised part e_{MB} acc. to eq. (6) it is possible to transfer the original calibration to any other gas as long as we stay inside the Reynolds range of our calibration data base.

2.3 Statistics of parameters for bearing friction

At PTB, there have been meanwhile 44 turbines evaluated with spin down and step response test covering a wide range of constructions (6 different types) and sizes (DN50 to DN400). Shows the outcome for the two parameters a_{20} and b_{20}.

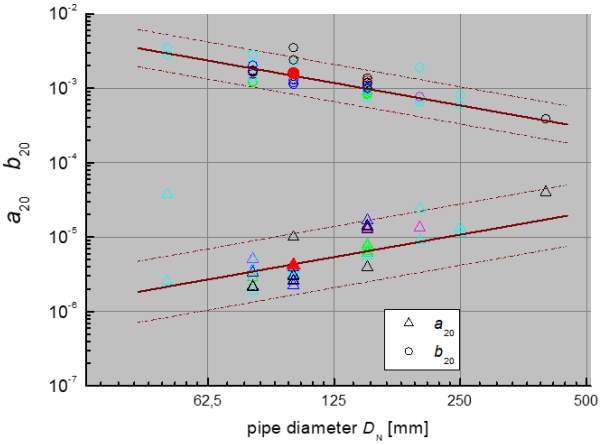

Figure 2: Statistic of parameters a_{20} and b_{20} for different turbine meters. In total there have been 44 turbine meters evaluated from 6 manufacturers (construction types), indicated by colour of symbols. The red full symbols are the parameters of the example shown in Figure 1. The lines indicate a linear mean on the log scale and its doubled standard deviation.

If a meter shall be calibrated for application in hydrogen at 9 bar(a)[5], the similar Reynolds number can be achieved with air at 1 bar with only 26% higher flow rates due to the other norm density and viscosity of hydrogen compared to air. So, if we make use of eq. (5)(6) to calculate the expected difference between calibrations result from 1 bar air and the application with 9 bar hydrogen, the part e_{Re} can be considered as similar and only the difference of the e_{MB} is significant. In Figure 3, we show the outcome for two sizes of meter using the averaged values of the parameters a_{20} and b_{20} from Figure 2.

As Figure 3 illustrates, the differences to the air calibration at 1 bar is the less the larger the meter is. It will be also the less the higher the density of the fluid will be. Hence, we can derive a general expectation that for most of the turbine meters with size larger than or equal to DN100, the application in hydrogen at 9 bar(a) and higher will be possible for a turn down ration of 1:10 or better.

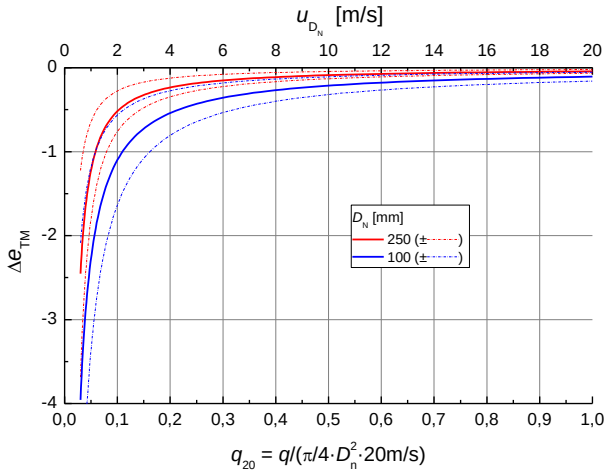

Figure 3: Predicted difference of meter deviations of TMs with D_N = 100 mm and D_N = 250 mm for usage in Hydrogen@9bar(a) when calibrated with air@1bar applying same Reynolds numbers for a certain flow rate. The parameters for bearing friction are taken from Figure 2 using the mean lines and related standard deviations.

3. Rotary Meters (RM)

3.1 Model for meter deviation of RM

The meter deviation of rotary meters has a similar background as turbine meters and the basic relation of torques at stationary condition is the starting point:

$$J\dot{\omega} = 0 = M_{\Delta p} + M_{\tau_W} + M_B \qquad (7)$$

The torque M_B due to bearing friction is again caused by the Newtonian fluid in the bearings and therefore also the simple linear relationship to rotation frequency resp. the indicated flow rate applies:

$$M_B = a_{mb} + b_{mb} q_i = C_B(a + q_i) \qquad (8)$$

As documented in [4], the characteristics of bearings in rotary meters are very close to that of turbine meters.

The main driving torque $M_{\Delta p}$ for rotary meters is given by the pressure difference across the piston Δp multiplied with the cross section A_{piston} of the piston acting at a certain lever $l_{\Delta p}$, so that we get:

$$M_{\Delta p} = A_{\text{piston}} \cdot l_{\Delta p} \cdot \Delta p = C_{\Delta p} \cdot \Delta p \qquad (9)$$

The third torque $M_{\tau w}$ in eq. (7) is the drag of the gap flow between the piston and the walls due to the wall shear stress τ_W at the tip surface of the piston. We consider a surface area $A_{\tau w}$ where the shear stress is acting (causing force) and the related lever $l_{\tau w}$ to establish the torque:

$$M_{\tau_W} = A_{\tau_W} \cdot l_{\tau_W} \cdot \tau_W = C_{\tau_W} \cdot \tau_W \qquad (10)$$

Finally, we have:

[5] We choose 9 bar(a) resp. 8 bar(g) for example because it is a representative pressure in local middle pressure supply networks.

$$0 = C_{\Delta p} \cdot \Delta p + C_{\tau_W} \cdot \tau_W + C_B(a + q_i) \qquad (11)$$

To find the relationship with the meter deviation, we make use of simplified relations of the gap flow as shown in Figure 4.

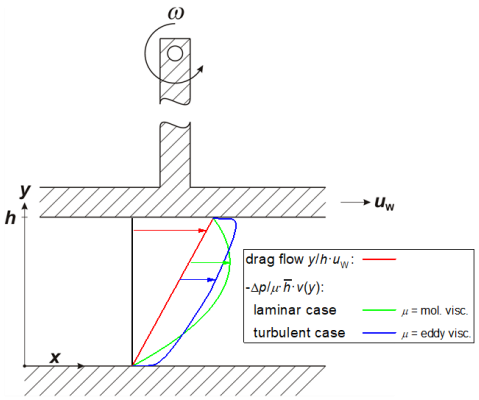

Figure 4: Schematic relations in a gap with one fixed and one moving wall (piston) with laminar and turbulent Couette flow (superposition of drag flow and flow driven by pressure difference).

The gap flow as shown in Figure 4 can be described as a Couette flow. It is a superposition of a drag flow and a flow driven by the pressure difference Δp across the piston. The basic formulation for the velocity across the gap is:

$$u(y) = \frac{y}{h} u_W - \frac{\Delta p}{\mu} \bar{h} \cdot v(y) \qquad (12)$$

what is valid for both, laminar as well as turbulent Couette flows. But we must consider that the Δp- driven part contains a term for viscosity which is the molecular viscosity $\mu_{\text{mol.}}$ in laminar case and the so-called eddy viscosity $\mu_{\text{eddy visc.}}$ in turbulent case[6]. The eddy viscosity is much higher than the molecular viscosity. It causes also large differences in the velocity profile shape in the gap. Therefore, we highlighted in red the parts strongly depending on Reynolds number in eq. (12) and in all equations below.

Next, we derive from eq. (12) the volume flow rate through the gap q_{gap} as an integral of velocity across the height h and with b of the gap:

$$q_{gap} = b \int_0^h \frac{y}{h} u_W - \frac{\Delta p}{\mu} \bar{h} \cdot v(y)\, dy \qquad (13)$$

where we can summarize parts into coefficients and considering that the wall velocity u_W of the piston tip is proportional to the flow rate q_i indicated by the RM:

$$q_{gap} = C_{gap,1} q_i + C_{gap,2} \frac{\Delta p}{\mu} \qquad (14)$$

The gap flow is directly related to the real flow q and the indicated flow q_i via an adjustment factor C_{just} (C_{just} is applied in practise to keep the meter deviation close to Zero):

$$q_{gap} = q - C_{just} q_i \qquad (15)$$

Further, the velocity profile as shown in Figure 4 allows also to derive a relationship for the wall shear stress τ_W:

$$\tau_W = -\mu \frac{\partial u}{\partial y}\Big|_{y=h} \qquad (16)$$

$$\tau_W = -\mu \left(\frac{u_W}{h} - \frac{\Delta p}{\mu} \bar{h} \cdot \frac{dv(y)}{dy} \right) \qquad (17)$$

$$\tau_W = \mu C_{\tau,1} q_i + C_{\tau,2} \Delta p \qquad (18)$$

Combining the equation (11) with (14), (15) and (18), we can substitute Δp in (11) with terms of real flow q and indicated flow q_i. Finally, all in all it can be reformed to get expression for meter deviation $e = q_i/q - 1$:

$$e_{RM} = \alpha_{Re} \left[1 + \hat{C}_B \frac{(a + q_i)}{\mu q_i} \right] + O_{just} \qquad (19)$$

$$\text{with } \alpha_{Re} = \frac{C_{gap,2} C_{\tau_W} C_{\tau,1}}{(C_{just} + C_{gap,1})(C_{\Delta p} + C_{\tau_W} C_{\tau,2})} \qquad (20)$$

3.2 Modelling of viscosity μ with transition from laminar to turbulent

As introduced in the explanations to eq. (12), we consider two different types of viscosity, depending on the laminar or turbulent state of boundary layer. Therefore, we need a modelling of the viscosity to express the actual viscosity in dependency on Reynolds number.

The molecular viscosity $\mu_{mol.}$ is a basic, physical parameter of the fluid and is in strict relation to the Reynolds number (as it is used in the definition of the Reynolds number):

$$\mu_{mol.} = \frac{4}{\pi D} \frac{\rho Q_i}{Re} \qquad (21)$$

The eddy viscosity $\mu_{eddy\ visc.}$ is not that well defined and is an increasing function of Reynolds number. We make use of the situation of full rough, turbulent flow and we can express the actual eddy viscosity with:

$$\mu_{eddy\ visc.} = C_{turb} \rho Q_i \qquad (22)$$

With this definition, the friction factor resp. wall shear stress τ_W in the Moody diagram is a horizontal line.

[6] Exactly: $\mu = \mu_{\text{mol.}} + \mu_{\text{eddy visc.}}$

We expect that the molecular viscosity and the eddy viscosity are equal at the transitional Reynolds number Re_{tr}, and we get:

$$C_{turb} = \frac{4}{\pi D}\frac{\rho Q_i}{Re_{tr}} \tag{23}$$

To keep the model equation (19) simple, we choose:

$$\begin{aligned} &if(Re < Re_{tr})\ \{\mu = \mu_{mol.}\};\\ &else\ \{\mu = \mu_{eddy\ visc.}\} \end{aligned} \tag{24}$$

3.3 Example for meter deviations of a RM

In Figure 5 we show for one rotary meter the meter deviations versus Reynolds number determined at PTB for a bigger span of metering conditions: the measurements with atmospheric air (black squares), with pressurized air up to 16 bar (symbols to indicate flow rates and colours to indicate pressure level) and measurements with natural gas (NG) at 17 bar and 50 bar (crosses).

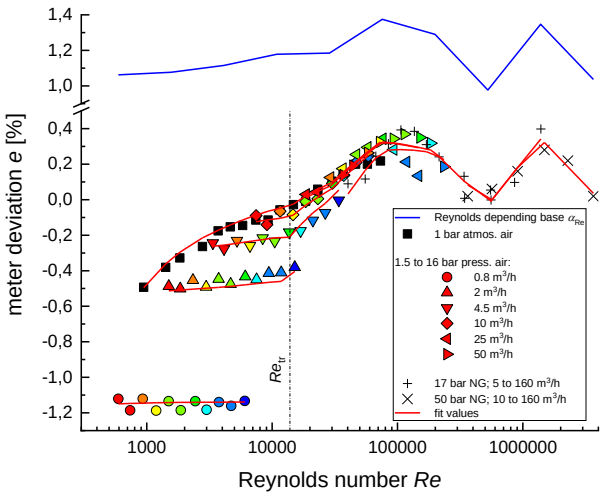

Figure 5: Meter deviations e of a rotary meter for various flow rates, pressures and fluids together with the Reynolds depending base curve α_{Re} and the fit curve according to eq. (19). For the parameters in eq. (19) beside α_{Re} see Table 1.

Additionally, to the single measurement results, the basic curve α_{Re} as a central part of eq. (19) is shown in Figure 5. Together with the other parameters (see also Table 1), we get the fit curve for meter deviation shown as red line.

It is relatively good to be seen in Figure 5 that for $Re < Re_{tr}$ (≈ 14000) the basic curve α_{Re} is nearly constant and the meter deviations at a fixed flow rate does also not depend on Reynolds number. In this area, the gap flow is behaving like a laminar flow and the meter deviations are dominated by $1/(\mu q)$ with $\mu = \mu_{mol.}$. This changes significantly when $Re > Re_{tr}$ and the gap flow is turbulent with $\mu = \mu_{eddy\ visc.}$. Due to the much higher value for $\mu_{eddy\ visc.}$ the term $1/(\mu q)$ is now much less important and the curve of meter deviation follows closely to the trend of the basic curve α_{Re} (in distant with the adjustment offset O_{just}).

Table 1: Parameters in eq. (19) for RM in Figure 5

Parameter	*value*
$\hat{C}_B$	-2.956e-6
a	0.0013
O_{just}	-1
Re_{tr}	13865

In Figure 6, we show the calibration values versus volume flow rate with atmospheric air and the expectation for hydrogen at 9 bar(a) based on the parametrisation of the meter investigated.

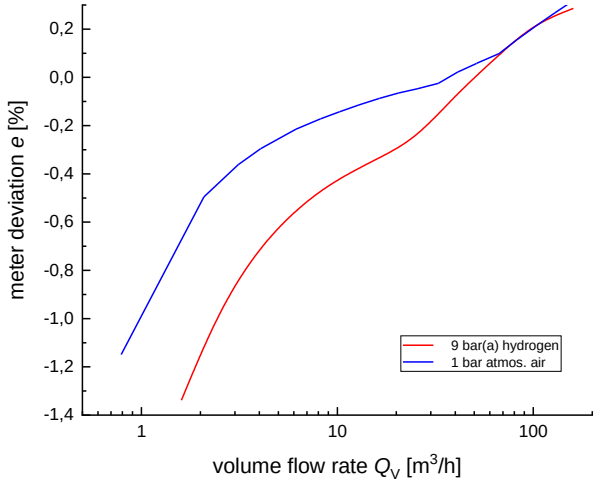

Figure 6: Meter deviation for meter of Figure 5 for atmospheric air and the expectation based on model eq. (19) for hydrogen at 9 bar(a).

The difference between air and hydrogen is significant at low flows while at higher flows this difference disappears (following the same argumentation for $1/(\mu q)$ above). But the impact of the fluid property is much less compared to that for turbine meters. The main reason is that for turbine meters the impact of bearing friction is scaled by $1/(\rho q^2)$, see eq. (6), while for rotary meters we have $1/(\mu q)$. With the ration of norm densities air to hydrogen of about 14:1 but ration of (molecular) viscosities of 2:1, it is understandable why the rotary meters react much less than turbine meters. A high-quality rotary meter with turn down ration of 1:160 with air can have still a turn down of 1:80 with hydrogen as the example shows in Figure 6.

4. Differential Pressure Meter (DPM)

Differential pressure meters like orifices [6], ISA and Venturi nozzles [7] as well as Venturi tubes [8] designed according to the ISO 5167 have from their physical principle a clear pure dependency on Reynolds number except a correction by means of the expansion number ε for compressible fluids. Therefore, the ISO5167 does not distinguish between different fluids but is valid for wide range of incompressible as well as compressible fluids and is implicitly including also pure hydrogen or blend of natural gas with hydrogen. The proof in practise for

equivalence between (hot) water and natural gas is documented for example in [5]. In this paper, we show in section 4.1 below exemplary measurement results of an orifice meter run applied in air, (cold) water, and natural gas.

One of the disadvantages of DPMs according to ISO 5167 is the dependency of the sensor signal Δp on a quadratic function of the measurand mass flow rate q_m. This sets high requirements on the Δp-measurement and limits the rangeability in practise to a level of normally not more than 1:10. With view to this aspect, laminar flow elements (LFEs) are more "efficient" due to the linear relationship between Δp and q_m, so that the rangeability is extend to 1:30. But it is difficult to maintain laminar flow in the LFE-matrix for higher pressures and flows. In section 4.2 we introduce to a special construction developed at PTB which allows to achieve laminar flow for hydrogen flow up to velocities of 4 m/s and pressure of 9 bar(a). The measurement results also demonstrate the continuous, smooth transition of the measurement behaviour $\Delta p = f(q_m)$ from laminar to turbulent.

4.1 Orifice meter according to ISO 5167-2 [6]

There have been 5 orifice runs designed and calibrated at PTB in the past 3 years with pipe sizes from 50 mm to 200 mm. Out of this set, we show the result of an DN150 orifice meter run which has been calibrated with air, water (ϑ = 20 °C), and natural gas. Some main characteristics are given in Table 2. Figure 7 shows the single measurement results.

Table 2: Characteristics of orifice meter with c_D-values shown in Figure 7

Pipe diameter D	146.3 mm
orifice diameter[7] d	62.15 mm
diameter ratio β	0.42481
pressure tapping	flange
Straight upstream length	13.5 D
Downstream length	4 D
Flow conditioner at Inlet	CPA 65

The Reynolds numbers achieved with (atmospheric) air and natural gas (NG) at 17 bar are overlapping around $Re = 10^5$. The additional test with water support just this range very well. The discharge coefficient c_D was the measurand and the calculation followed in all details as described in [6]:

$$c_D = \frac{q_m\sqrt{1-\beta^4}}{\varepsilon\frac{\pi}{4}d^2\sqrt{2\rho_1\Delta p}} \qquad (25)$$

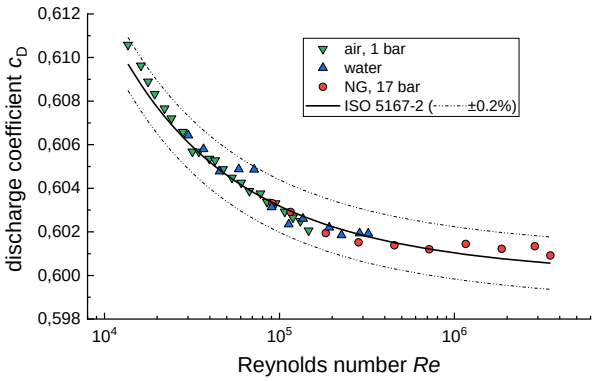

Figure 7: Calibration results of an orifice meter with nominal pipe size of D_N = 150 mm in comparison with the reference curve of ISO 5167-2 [6]. For further parameters see Table 2.

As one can obtain in Figure 7, the set of single results are in an agreement with the c_D documented in [6] within a span of ±0.2%. This is a remarkable good agreement when taken into account that there have been applied three different test rigs (i.e. installation conditions) and three different sets of auxiliary sensor equipment (for Δp, absolute pressure and temperature). The results of Figure 7 is also exemplary the other four orifice runs investigated at PTB in the past three years.

4.2 DPM based on porous matrix

The challenge to keep laminar flow in LFEs for higher volume flow rates at higher pressures initiated at PTB the development of a special DPM in which a porous matrix is applied to establish the differential pressure, see Figure 8. Flows through porous media are extensively described mainly in geological science (for underground flow of fluids) and can be found under the key words Darcy- or Forchheimer flow.

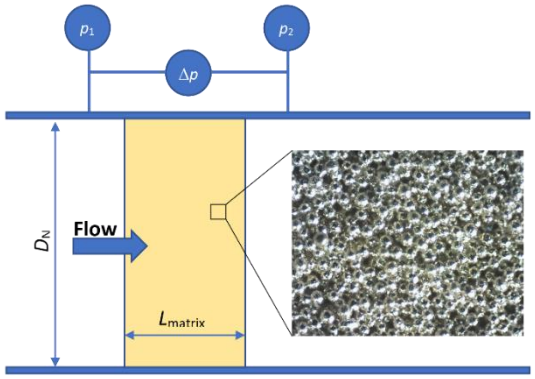

Figure 8: Schematic construction of a DPM with a porous matrix as central part to establish differential pressure Δp. The photo of the porous matrix is of the material B40 (see Table 3).

During the testing of this concept at PTB, we applied different materials with various sizes of pore diameter, length of matrix, and pipe diameter as well as different conditions of measurement (pressure and gas). The materials and test conditions are listed in Table 3.

[7] It must be noted that the originally value of the orifice diameter was d = 62 mm from design process. With this value we obtained a constant offset against the ISO curve of 0.4 %. The correction to d = 62.15 mm is arbitrary but lies within the manufacturing tolerances.

Table 3: Characteristics of test items with porous material. The nomenclature of the materials is given by the manufacturer SIPERM GmbH.

Material ID	d_{pore} [µm]	L_{Matrix} [mm]	D_N [mm]	**fluid**	**press.** [bar]
HP10	16	4.5 / 10	100	air	1
HPFI	50	20	30	air	1 .. 2.3
HP80	78	5 /10 /15	100	air	1 .. 16
B40	33	10 /21	17 /150	air + NG	1 / 17

To evaluate all the results gathered with such different conditions with focus on general conclusions, we make use of the definitions for the friction factor c_f as a normalised differential pressure (eq. (26)), and the Reynolds number Re_{pore} (eq. (27)), using the flow velocity u_{pore} inside of the matrix and the pore size d_{pore}.

$$c_f = \frac{\Delta p}{\rho_1 u_{pore}^2} \frac{d_{pore}}{L} \left(1 + \frac{p_2}{p_1}\right) \tag{26}$$

$$Re_{pore} = \frac{\rho_1 u_{pore} d_{pore}}{\mu} \tag{27}$$

The summarized outcome of all experiments can be seen in Figure 9. The single measurements results are following the trend of laminar flows ($c_f \sim 1/Re_{pore}$) for small *Re*-numbers and the trend of turbulent flows ($c_f \sim 1/Re_{pore}^{1/7}$) for high *Re*-numbers. Around $Re_{pore} = 10$, we can obtain a continuous, smooth transition between both states of flow. With this, we have a compact and robust device where we can use the advantage of $\Delta p \sim q_m$ below $Re_{pore} = 10$ but we can go also to higher ranges having smooth curve versus Reynolds number.

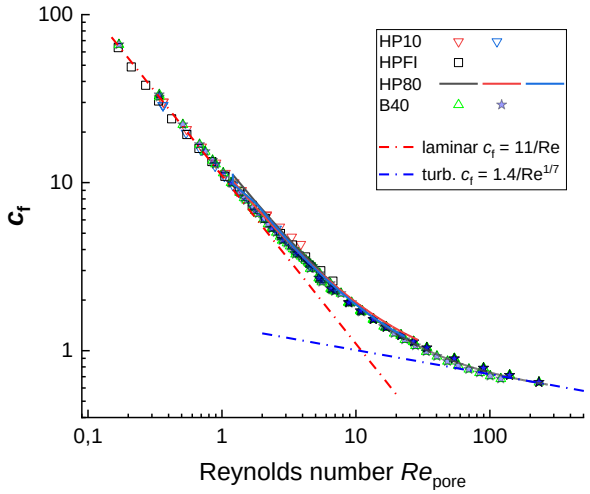

Figure 9: Normalised pressure loss (friction factor) c_f (eq. (26)), versus Reynolds number (eq. (27)) for different porous materials, see also Table 3.

The value of $Re_{pore} = 10$ seems in the first moment quite low but it is that small due to the pore size in the magnitude of 10 to 100 µm. To get a realistic impression, following situation should illustrate the operation conditions: using the material B40 (Table 3) and a velocity of u_{pore} = 4 m/s, we achieve the transitional $Re_{pore} = 10$ with pure hydrogen at 9 bar(a). The flow velocity in the main pipe outside of the matrix is approx. 1.7 m/s what ends up with a volume flow rate of $q \approx 100$ m^3/h for a pipe size of DN150. Hence, this construction is a reasonable approach for a check meter when e.g. a rotary meter of size G65 is used as working standard.

5. Conclusion and outlook

The main intension of the paper was to introduce to the approaches at PTB to establish reliable transferability of calibrations gathered with conventional test fluids like air or natural gas to applications with pure hydrogen or blend with hydrogen. The transferability for all meter types discussed in this paper is based on a Reynolds similarity but for each meter type specific deviations from pure Reynolds similarity have been taken into account.

The details of the mathematical models for the mechanical meters (turbines and rotary meters) have been explained and examples have been shown which underlay the general outcome. Essential point for the transferability of the calibration values of mechanical meters is the reliable modelling and parametrisation of the bearing friction which causes the main deviations from a pure Reynolds dependency. With the examples (and in case of turbine meters by means of statistics), the potentials of these meters have been discussed with view to the rangeability in volume flow rate. The elaborated rangeability of 1:10 for turbine meters and 1:80 for rotary meters as a minimum for applications in 9 bar(a) pure hydrogen is confirming that these meter technologies are still reasonable applicable for such applications. The situation for hydrogen at higher pressures will be better due to the higher densities and higher Reynolds numbers.

In section 4, the usage of orifice meter runs constructed according [6] has been illustrated by calibration results. The long-term experience behind [6] ensures a high level of transferability between incompressible as well compressible fluids in a wide range what could be underfed again with discharge coefficients experimentally determined at PTB.

A new construction of DPM was presented which was designed at PTB to extend the range of LFE-behaviour to higher pressures and higher flow rates. It is based on the usage of porous materials with pore sizes between 10 and 80 µm. At least for applications in the middle pressure range with hydrogen it provides a good alternative for a check meter in series with conventional rotary meters.

All exemplary results shown in this paper demonstrate that a basic uncertainty of the transferable calibration values in the order of 0.2 % is achievable. With additional sources of uncertainty when such meters are applied for providing traceability on site, we expect a total uncertainty in the order of 0.3 % or better. It has to be

emphasized that this level of uncertainties needs the individual determination of meter characteristics based in a wider range of calibrations, i.e. wide range of Reynolds number using different calibration pressures and in case of turbine meters the application of specific tests (spin down and step response).

The activities of PTB to establish traceability at the test facilities at DNV and RMA for pure hydrogen are in progress parallel to the publication of this paper. All the approaches presented in this paper are in application there, so that it is expected to have confirmation based on larger set of experimental results gathered with pure hydrogen until end of this year latest.

References

[1] Mickan B, van der Grinten J, Kappes T, "Primary and secondary flow standards for a wide variety of gas compositions - a solid base for reliable traceability facing the energy transition". *38th North Sea Flow Measurement Workshop*, Virtual Conference, 27-29 October, 2020, https://tinyurl.com/fyyb9zh5

[2] Van der Grinten J, Gunnarsson A., Van der Beek M, Mickan B., "An intercomparison between primary high-pressure gas flow standards with sub-permille uncertainties". *37th International North Sea Flow Measurement Workshop*, 22-25 Oct 2019, Norwegian Society for Oil and Gas Measurement.

[3] Van der Grinten J et al., "Gas flow traceability for non-conventional and renewable gases*", 39th North Sea Flow Measurement Workshop*, Tønsberg, Norway 26–29 Oct, 2021

[4] Böckler H B: *Messrichtigkeit von mechanischen Gasmessgeräten bei Verwendung von unterschiedlichen Gasbeschaffenheiten*", Band 101 von PTB-Bericht / Mechanik und Akustik, Physikalisch-Technische Bundesanstalt, ISSN 0179-0595; Fachverlag NW in Carl Ed. Schünemann KG, 2019

[5] Van der Grinten J et al., "*An Intercomparison of Water Flow and Gas Flow Laboratories using ISO 5167 Dp Devices*", FLOMEKO 2016, Sydney, Australia, September 26-29, 2016

[6] ISO 5167-2: *Measurement of fluid flow by means of pressure differential devices inserted in circular-cross section conduits running full — Part 2: Orifice plates*, 2003.

[7] ISO 5167-3: *Measurement of fluid flow by means of pressure differential devices inserted in circular-cross section conduits running full — Part 3: Nozzles and Venturi nozzles*, 2003.

[8] ISO 5167-4: *Measurement of fluid flow by means of pressure differential devices inserted in circular-cross section conduits running full — Part 4: Venturi tubes*, 2003.